Pharm Res (2011) 28:82–94
DOI 10.1007/s11095-010-0122-x

RESEARCH PAPER

Formation and Closure of Microchannels in Skin Following Microporation

Haripriya Kalluri • Ajay K. Banga

Received: 6 September 2009 / Accepted: 8 March 2010 / Published online: 31 March 2010

ABSTRACT

Purpose To characterize the microchannels created in hairless rat skin by microneedles and investigate their closure following exposure to different occlusive conditions.

Methods Maltose microneedles were characterized by scanning electron microscopy. The microchannels created and their closure when exposed to different conditions was investigated using a variety of techniques.

Results Microscopic imaging indicates a pyramidal geometry of maltose microneedles with an average length of 559 ± 14 μm and tip radius of 4 μm. Upon insertion into skin, they created microchannels with an average surface diameter of 60 μm and an average depth of 160 ± 20 μm as observed by histological sectioning and confocal microscopy. Skin recovers its barrier function within 3–4 hrs, and microchannels closed within 15 hrs of poration when exposed to environment. However, when occluded, the microchannels remained open for up to 72 hrs *in vivo*, as observed by calcein imaging, transepidermal water loss measurements and methylene blue staining.

Conclusion Maltose microneedles penetrated the stratum corneum barrier and created microchannels in skin which completely close within 15 hrs after poration. However, under occluded conditions, barrier recovery can be delayed for up to 72 hrs *in vivo*.

KEY WORDS microchannels · microneedles · microporation · pore closure · transdermal delivery

H. Kalluri • A. K. Banga (✉)
Department of Pharmaceutical Sciences,
College of Pharmacy and Health Sciences, Mercer University,
3001 Mercer University Drive,
Atlanta, Georgia 30341, USA
e-mail: banga_ak@mercer.edu

INTRODUCTION

Transdermal Drug Delivery (TDD) is an appealing alternative to avoid the disadvantages associated with oral and parenteral administration of drugs. Transdermal delivery allows the permeation of drugs across the skin and into the systemic circulation, thus avoiding the hepatic first-pass effect observed for oral administration and the inconvenience of frequent parenteral administration. However, the permeation of compounds is limited to small, lipophilic molecules due to the outermost skin barrier, the stratum corneum (SC). Stratum corneum is a biphasic layer with both hydrophilic and hydrophobic regions; it maintains the hydration levels of skin and simultaneously acts as a barrier to foreign materials. Several chemical and physical enhancement techniques, such as iontophoresis, ultrasound/sonophoresis, microneedles, electroporation, laser ablation and chemical enhancers, have been explored to overcome the stratum corneum barrier and, in turn, increase skin permeability. Microporation techniques employed in transdermal drug delivery, such as microneedle technology, thermal and radiofrequency ablation, laser ablation and other combination approaches, have been recently reviewed (1).

Microneedle technology offers a cost-effective, minimally invasive, and controllable approach to transdermal drug delivery. It involves the creation of micron-sized channels in the skin, thereby disrupting the stratum corneum barrier. Upon creation of the microchannels, interstitial fluid fills up the channels, resulting in hydrophilic pathways. As indicated by recent literature, there has been an increased interest in this technology, and a wide range of drug moieties, including hydrophilic compounds and macromolecules, have been shown to be delivered transdermally (2–13). For example, Wang *et al.* have reported a 25% decrease in blood glucose levels upon administration of insulin via

hollow microneedles (14). In another study, Cormier *et al.* employed desmopressin-coated solid microneedles to deliver 20 μg of the drug across hairless guinea pig skin within 15 min of application (3). Studies related to various aspects of microneedle technology, such as fabrication of microneedles, types of microneedles (solid/hollow), TDD via microneedles, delivery of microparticles, insertion kinetics of microneedles, human studies, lack of pain associated with microneedles, pore closure and combination approaches, have been recently reviewed by us (15).

A wide range of microneedle designs have been applied to solid/hollow microneedles for applications in transdermal drug delivery, and studies have been reported on the effect of geometrical parameters on drug delivery. Teo *et al.* studied the effect of microneedle diameter on drug delivery. From *in vitro* studies, they reported that while microneedles with a diameter of 50 μm increased delivery by 10-fold, microneedles with a diameter of 150 μm further increased permeation levels upto almost 20-fold (13,16). This could be attributed to larger pores created by microneedles with a bigger diameter. Microneedle length is another major factor that will influence the depth of the created pores, drug delivery and recovery time. Oh *et al.* reported that an increase in microneedle length from 200 μm to 500 μm resulted in a ~5-fold increase in permeation levels, *in vitro*. Microneedle density also affected permeation levels with a linear increase in permeation levels (17). However, a densely packed microarray with less needle-to-needle spacing distance may play a critical negative role in drug delivery due to the possibility of bed-of-nails effect (16,18).

Most of the literature on microneedle technology is focused on fabrication technologies or drug delivery, and not many studies have been reported on the basic aspects of microporation, such as characterization of microchannel dimensions and, especially, their closure. When the skin barrier is disrupted, skin repair starts immediately due to the stimulation of the lamellar bodies in the skin (19). Microporation compromises barrier integrity, and the microchannels created by microneedles usually reach into the viable epidermis, thus resulting in an increase in transepidermal water loss (TEWL). It has been reported that this imbalance in skin hydration levels stimulates the lamellar bodies in the skin to start the healing process (20). However, the recovery time for the healing process depends on the degree of barrier disruption, which, in turn, depends on the geometry and dimensions of the employed microneedles. Therefore, it becomes important to study these parameters when designing a microneedle-based patch. Al-Qallaf and Das investigated the effect of various parameters, such as microneedle geometry, sharpness of tip, surface area of patch and skin thickness, on drug delivery (21). The effect of microneedle length, cross-section and microneedle density were also reported by Gupta *et al.*, who employed skin impedance measurements to study the time taken for the skin to regain normal function after microporation (in human volunteers). They reported that the healing time of skin greatly depended on the length of microneedles, cross-section of the employed microneedles and microneedle density (22,23).

As discussed earlier, considerable numbers of studies have been published pertaining to microneedle technology in transdermal drug delivery. However, pore closure has not been well characterized. Haq *et al.* have indicated the closure of microchannels at 24 hrs in human volunteers by superficial staining of skin and transepidermal water loss measurements at set time points (24). Also, as mentioned earlier, Gupta *et al.* have employed skin impedance measurements to study skin healing after application of microneedles with different geometrical parameters, under both occluded and non-occluded conditions (22). However, these studies did not include direct visualization of this healing phenomenon. Therefore, in these studies, for the first time, we have comprehensively studied and reported pore closure by various techniques, such as calcein imaging, transepidermal water loss measurements and methylene blue staining. We have also studied the effect of formulation pH and different occlusive conditions on pore closure.

MATERIALS AND METHODS

Materials

Maltose microneedles (500 μm) were obtained from Elegaphy, Inc. (Otsu, Japan). Each array consists of three stacked layers of microneedles; each layer in turn has 27 soluble microneedles which dissolve upon insertion into skin. Fluoresoft (0.35%)® used in calcein imaging studies was obtained from Holles Laboratories Inc. (Cohasset, MA, USA). FluoSpheres® (0.2 μm) were obtained from Invitrogen™ (Carlsbad, California, USA). Methylene blue dye used in dye binding studies was obtained from Eastman Kodak Co. (Rochester, NY, USA).

Male hairless rats, the animal model for these studies, were obtained from Charles River Laboratories (Wilmington, MA, USA) and were housed in the Mercer University animal facility until use. All the animal studies were reviewed and approved by the Mercer University Institutional Animal Care and Use Committee.

Methods

Characterization of Microneedle Dimensions by SEM

Geometry and dimensions of maltose microneedles were studied using a Hitachi S-4100 scanning electron micro-

scope (SEM; Hitachi High-Technologies, Maidenhead Berkshire, UK). The microneedle array was directly placed in a field emission SEM at an accelerating voltage of 15 keV without any further coating. Images were taken at various magnifications to observe the geometry, and the actual length, base width and tip radius (sharpness) of the microneedles were measured using Vantage 1.3 software (Noran systems).

Characterization of Microchannels Created by Soluble Microneedles

Dye binding studies were performed to visualize the creation of microchannels by maltose microneedles. Freshly excised hairless rat skin, excised immediately after sacrifice, was obtained, and three line maltose microneedles were manually inserted, followed by staining with 1% (w/v) methylene blue dye solution for 1 min. The site was then cleaned with kimwipes and alcohol swabs to remove excess dye. Images were then taken with a Proscope HR video microscope.

Confocal microscopy studies were performed to characterize the depth and surface diameter of the microchannels. Skin from the abdominal region of hairless rats was obtained and porated with maltose microneedles. FluoSpheres® (0.2 μm) were applied for 20 sec, after which excess was removed with kimwipes. The sample was then placed on a slide and mounted onto a Zeiss confocal microscope. X-Z sectioning was performed at an excitation/emission wavelength of 495 nm/515 nm, respectively. The depth of the microchannels was investigated indirectly by the depth of permeation of the microparticles. The surface diameter of the microchannels was also measured using the LSM image browser software.

Histological sectioning was also performed to confirm the creation and depth of the microchannels. Hairless rats were anesthetized using ketamine (70 mg/kg) and xylazine (30 mg/kg). An area on the abdomen of the rat was treated with maltose microneedles, and the site was stained with methylene blue dye, after which the site was cleaned with alcohol swabs and kimwipes. The rat was then sacrificed by carbon dioxide asphyxiation, and the porated site was excised immediately and fixed in OCT compound medium (Tissue-Tek®). The blocks were instantly frozen using liquid nitrogen and were stored at −80°C until further analysis. Using a Microm HM 550 cryostat, 10 μm thick cryosections of the skin sample were cut and placed on a glass slide. The presence of the created microchannels was observed as a function of the depth from the surface layer (stratum corneum) of the skin, as indicated by the dye. Images were taken using a Nikon Eclipse E600 camera, attached to a microscope.

Different Occlusive Conditions Tested to Check for Any Effect on Pore Closure

Microneedle-treated sites were subjected to different occlusive conditions to investigate the effect of occlusion and pH on pore closure. The porated sites were either exposed to the environment (open site), exposed to citrate buffer (pH 4), exposed to phosphate-buffered saline (PBS) (pH 7.4) or occluded with a water-vapor impermeable plastic film (single-coated polyethylene medical tape; 3M 1521, 3M Pharmaceuticals). Studies were also performed to study pore closure when occluded with distilled water or buffers (Fig. 1).

Assessment of Barrier Integrity as Indicated by Transepidermal Water Loss (TEWL)

Hairless rats were anesthetized, and an area on the abdomen was cleaned with kimwipes. A VapoMeter® (Delfin Technologies Ltd., Kuopio, Finland) was employed to measure the change in transepidermal water loss (TEWL) after treatment with maltose microneedles. The VapoMeter® consists of sensors which measure the % RH (relative humidity) and convert it to a value representative of TEWL (g/m^2hr). Measurements recorded before microporation were considered as base values indicative of unperturbed skin barrier. TEWL measurements were taken again immediately after microporation and served as controls indicating open pores. To study the time taken for the skin to regain its normal barrier function, TEWL values were taken periodically over a period of time until the values fell back to base values.

In studies to check the effect of different test conditions on pore closure, the microneedle-treated sites were either left open to the environment, occluded with a plastic film or occluded with a solution. A liquid reservoir patch was used for occluding the porated sites with respective buffer solutions or water (Fig. 1). The patch consists of a plastic backing layer, reservoir chamber and adhesive layer. The

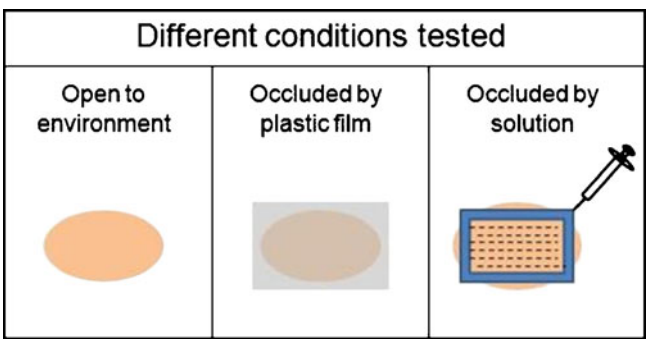

Fig. 1 Schematic of different conditions tested to check for effect on pore closure: (**a**) open site; (**b**) occluded by a plastic film; (**c**) occluded with solution.

respective solution was injected into the reservoir chamber. After 24 hrs, the site was cleaned with a kimwipe, and TEWL measurements were taken again to study presence or absence of pores. The sites were also stained with methylene blue dye for visualization of microchannels. The same procedure was repeated for checking the presence of microchannels at 72 hrs after microporation. As a control for this study, intact sites (without microneedle treatment) were occluded with plastic film and distilled water. TEWL values were measured at 24 hrs and 72 hrs after occlusion. ANOVA (analysis of variance; $p<0.05$) and t-test ($p<0.05$) were performed to analyze the data.

Calcein Imaging to Study Kinetics of Pore Closure

Calcein imaging studies were performed to study the kinetics of pore closure in microneedle-treated hairless rat skin. Hairless rats were anesthetized, and several areas on the abdomen were treated with microneedles. Calcein, a fluorescent dye (with excitation/emission wavelengths of 495 nm/515 nm), was applied to the treated sites at different time points of 0.25, 0.50, 1, 2, 3, 6, 8, 12, 15 and 24 hrs after poration. The site was then wiped with kimwipes to remove excess dye. A fluorescent image was taken that shows the distribution of fluorescence in and around each pore. The imaging system has been discussed by us previously. Briefly, it comprises a digital camera (Canon, USA) fitted with a macro lens attached in front with a 525 nm long pass filter (2).

To check the effect of different occlusive conditions on pore closure, the same procedure was employed. After exposure to the respective test conditions for 24, 48 and 72 hrs, fluorescent images were taken to investigate the presence of microchannels and the distribution of calcein. The images were processed using Fluoropore software, an image analysis tool, which measures the fluorescent intensity in and around each pore to give a value called the pore permeability index (PPI). This PPI value is representative of calcein flux into the skin for each pore. PPI values therefore indicate the creation of pores and their uniformity. In studies on the complete closure of pores under occluded conditions, treated sites were occluded with a plastic film, and calcein imaging was performed at 0, 72 and 120 hrs from the time of poration.

RESULTS

Characterization of Microneedle Dimensions by Microscopic Imaging

Scanning electron microscopy indicates a pyramidal geometry of maltose microneedles (Fig. 2a). Fig. 2b is a magnified image of a single microneedle showing its sharp tip. Microneedles had an average length of 559 ± 14 μm, an average base width of 213 ± 12 μm and a sharp tip with an average radius of around 4 μm. The sharp tips of these microneedles aid in effectively overcoming the stratum corneum barrier.

Characterization of Microchannels Created by Soluble Microneedles

Maltose microneedles, upon insertion into skin, effectively created microchannels as indicated by methylene blue staining (Fig. 3). Three line maltose microneedles created 81 microchannels—about 125 microchannels per sq. cm. Confocal microscopic images indicated the diffusion pathway of the microparticles across microporated skin. Fig. 4 shows the diffusion of the FluoSpheres® which upon application filled the microchannel pathway. The fluorescent microparticles penetrated up to an average depth of 160 μm±20 μm, thus indirectly indicating the depth of the created microchannels. They had an average surface diameter of about ~60 μm. This was further confirmed by histology studies. Histological sectioning of skin samples fixed immediately after poration indicated that the micro-

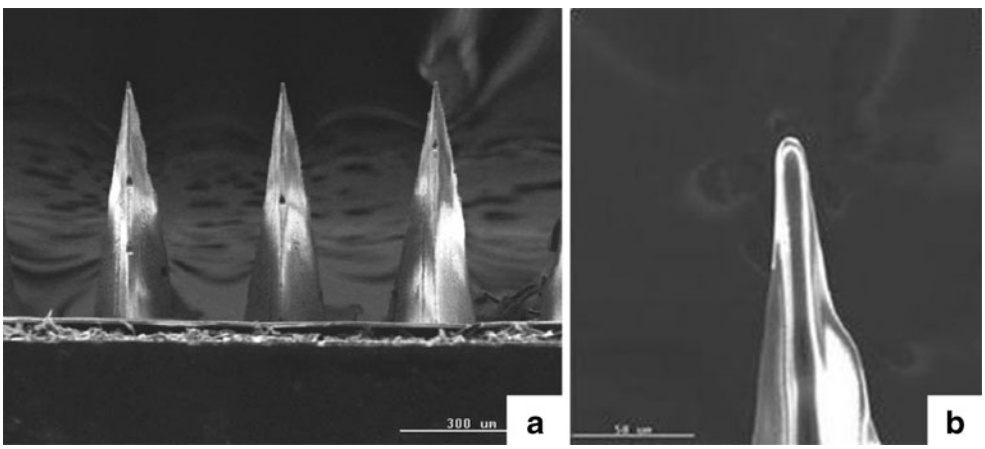

Fig. 2 Scanning electron microscopic images of maltose microneedles; (**A**) 40X magnification showing an array of microneedles: (**B**) 500X magnification showing the tip of a single microneedle with an average tip radius of ~4 μm.

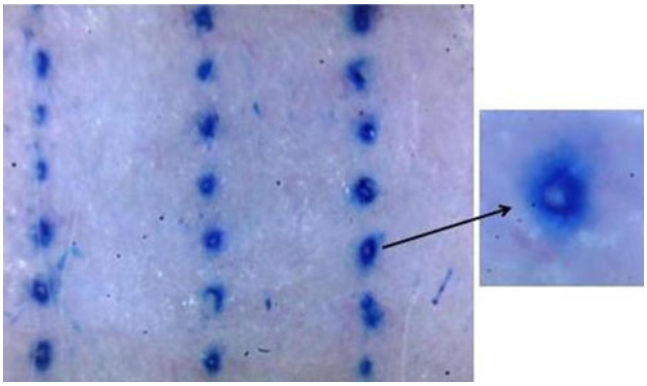

Fig. 3 Methylene blue staining for visualization of microchannels: (**a**) stereomicroscopic image showing three rows of microchannels and (**b**) a single microchannel. The *arrow* indicates a single microchannel.

channels created by ~560 μm long soluble microneedles have an average depth of 160 μm±20 μm (Fig. 5a–e).

Assessment of Barrier Integrity as Indicated by Transepidermal Water Loss (TEWL)

Transepidermal water loss was measured to study the time taken by the skin to regain normal barrier function. The increase in TEWL following barrier disruption is reported as the percentage increase from base values (of intact skin). Following microporation, there was more than 150% increase in TEWL values, which significantly decreased within the first 5 min. Following that, TEWL values gradually decreased and reached base values over a period of 4 hrs (Fig. 6), indicating that skin had regained its barrier function at the end of the experimental time period. Increase from the base value, immediately after microporation, may differ slightly from study to study. However, the variability of increase is not significant, as this just indicates the increased water loss from the site immediately after poration. The water loss decreases quickly enough to a point, after which it takes a while to decrease further to the base point.

In studies to check the effect of different test conditions on pore closure, intact skin had an average base value of 9.19±0.95 g/m^{2}hr, which increased to 18.67±1.86 g/m^{2}hr immediately after microporation. After 24 hrs, the TEWL values fell back to 10.60±0.46 g/m^{2}hr for the open site, indicating absence of micropores. However, for sites, occluded with a plastic film, TEWL values remained high at 18.77±0.90 g/m^{2}hr even at 24 hrs, thus indicating

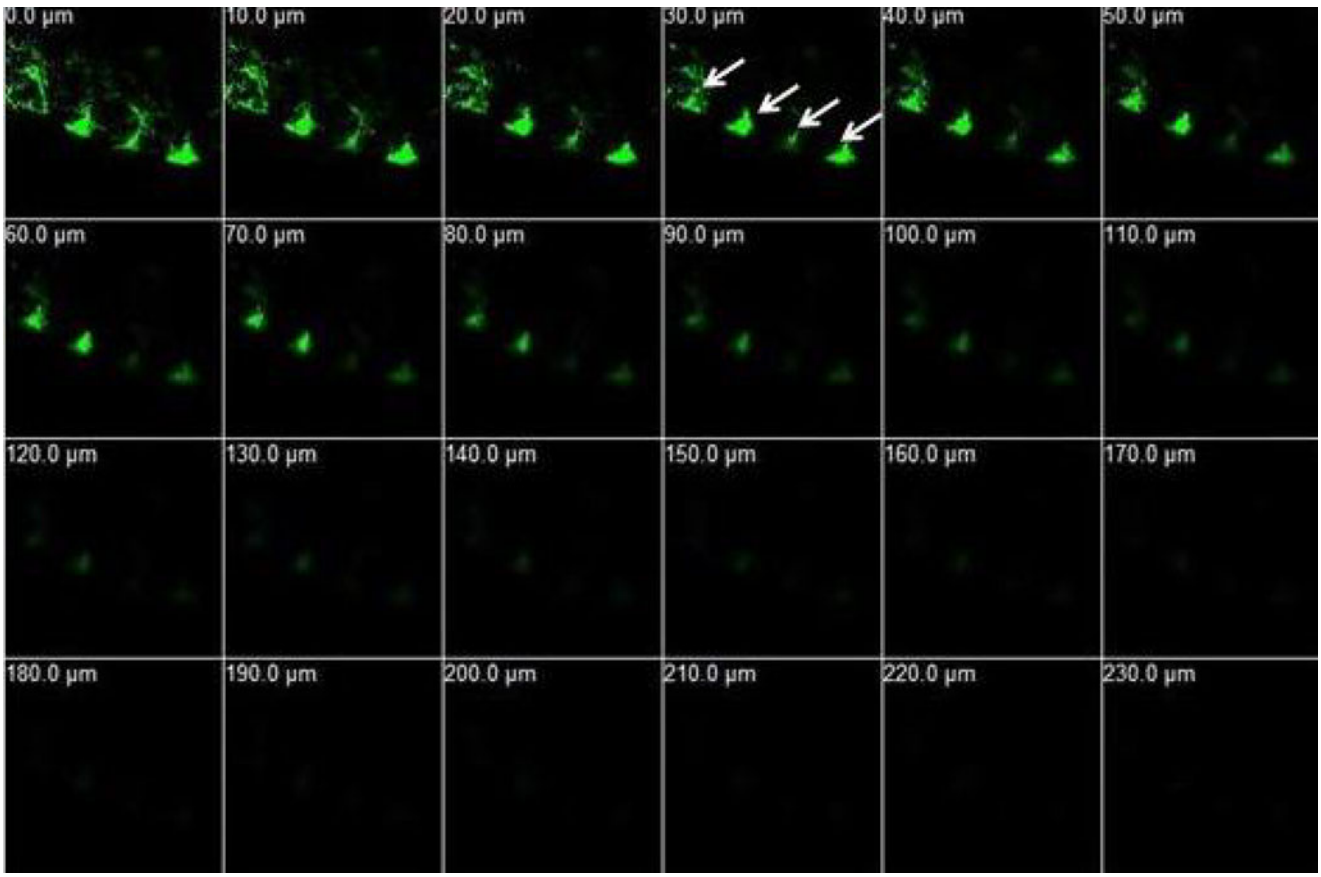

Fig. 4 Confocal microscopy to study depth of microchannels. The images indicate the permeation profile of 0.2 μm-sized fluorescent microparticles (FluoSpheres®) across hairless rat skin. Fluorescence was imaged up to an average depth of 160±20 μm, indicating the depth of the microchannels.

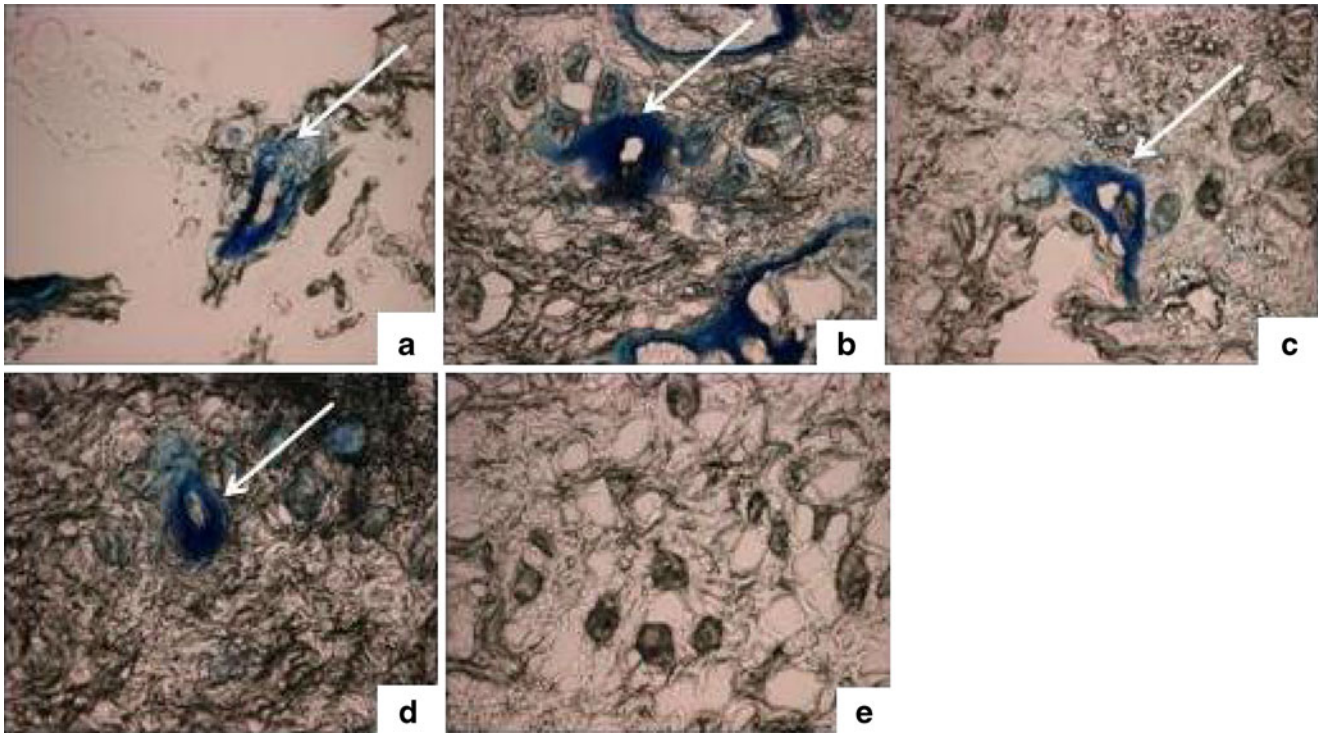

Fig. 5 Horizontal histological sectioning to check the presence of microchannels in microneedle-treated skin. Histological sections of treated skin fixed immediately after microporation: (**a**) top layer of skin, (**b**) at 90 μm deep, (**c**) at 120 μm deep, (**d**) at 160 μm and (**e**) at 200 μm from the surface of the skin. The *arrows* indicate a single microchannel (stained by methylene blue dye).

presence of micropores. Similar results were observed for sites exposed to both citrate and phosphate buffers (Fig. 7A). The presence of microchannels was further confirmed by methylene blue staining at the end of the experimental time. For the sites occluded with buffers or a plastic film, microchannels were visualized even at 24 hrs after microporation. However, no microchannels were observed for the sites exposed to the environment (Fig. 7A: (i–iv)).

A similar trend was observed for the 72 hrs time point as well (Fig. 7B), indicating that pores remain open up to 72 hrs *in vivo* upon occlusion. Similar results were obtained when the pores were exposed to distilled water as well (data not shown). These results indicate that pores remained open under occlusive conditions, and pH did not seem to have an effect on pore closure.

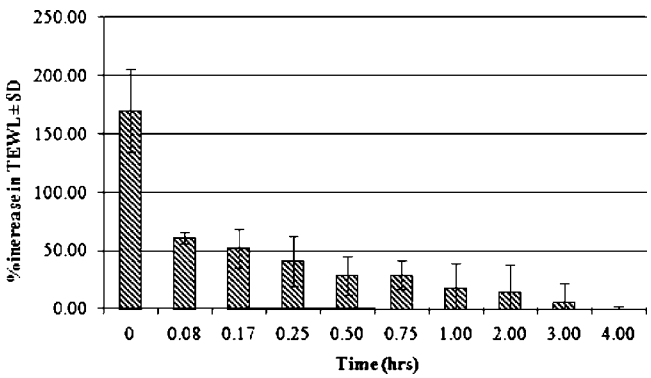

Fig. 6 Transepidermal water loss measurements to study recovery of barrier function in microneedle-treated skin. TEWL values are reported as percentage increase from base values of intact skin. *Error bars* indicate standard deviation (± SD).

Control study with untreated, occluded sites indicated that occlusion does increase TEWL slightly by 24 hrs and 72 hrs (average values of 12.93 g/m^2.hr and 13.27 g/m^2.hr, respectively). However, statistical analysis indicated that the values obtained for control are statistically lower than those obtained for the porated and occluded sites at 24 hrs (p= 0.002) and 72 hrs (p=0.038). Similar results were obtained for porated sites which were occluded by water or buffers at both 24 and 72 hrs time points (data not shown).

Calcein Imaging to Study Kinetics of Pore Closure

Fluorescence imaging was employed to study pore closure when exposed to the different test conditions. The time taken for the pores to close when exposed to the environment was investigated by calcein imaging at different time points from the time of poration. Fig. 8a is a fluorescent image of intact skin which shows background fluorescence. Images taken immediately after microporation indicate permeation of calcein through the microchannels as indicated by increased fluorescence intensity (Fig. 8b). At 12 hrs after poration, there was faint

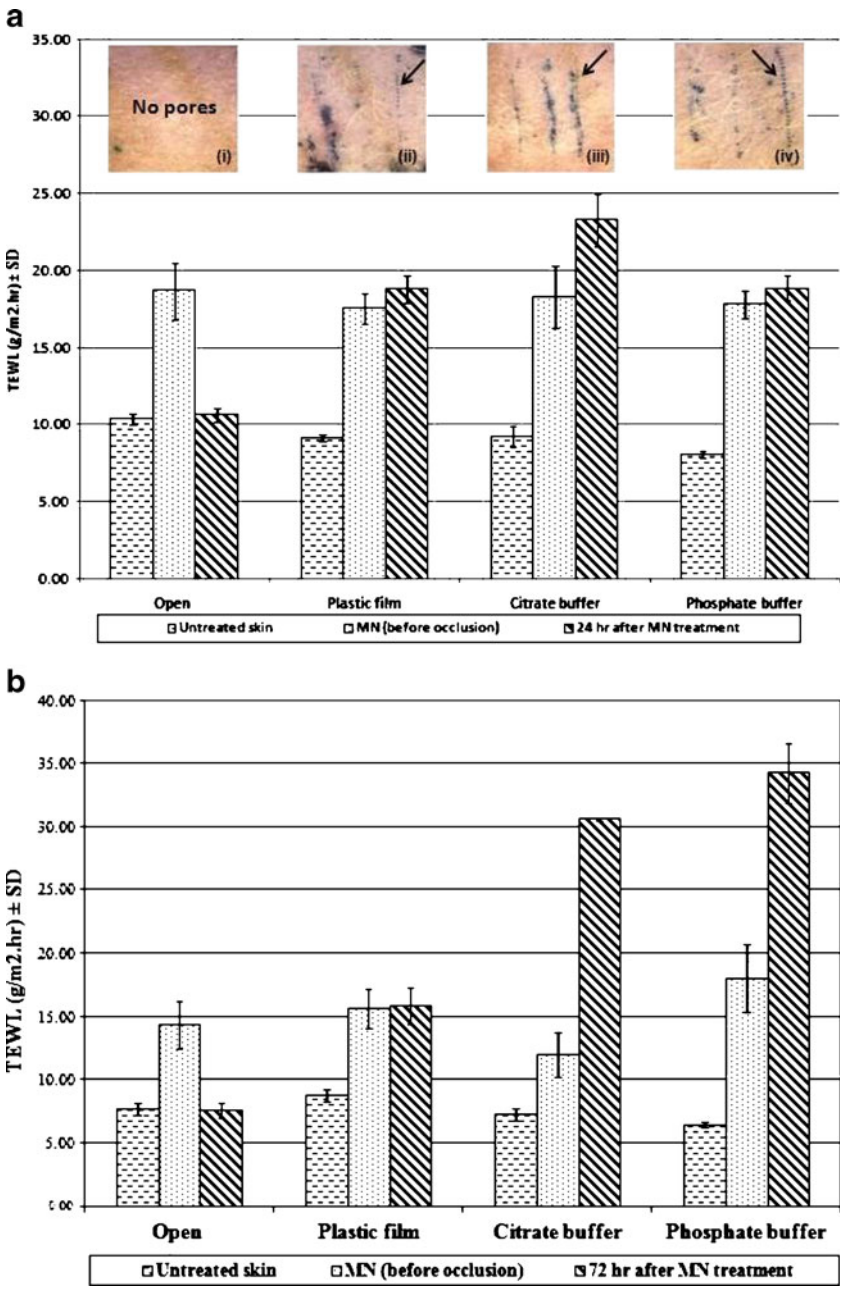

Fig. 7 Transepidermal water loss measurements to assess pore closure at (**A**) 24 hrs and (**B**) 72 hrs, after microporation ($n = 4$). In both cases, microchannels closed when exposed to the environment as indicated by low TEWL values. However, they remained open under occluded conditions (plastic film, citrate buffer, PBS buffer) as indicated by high TEWL values. This was further confirmed by methylene blue staining (i–iv). The *arrows* in (ii–iv) indicate presence of microchannels. *Error bars* indicate standard deviation (± SD).

fluorescence indicating partially open pores (Fig. 8f). However, by 15 hrs, the pores closed as seen in Fig. 8g.

When microneedle-treated sites (Fig. 9a) were occluded with water or a plastic film, pores remained open at 24 hrs *in vivo* (Figs. 9c & d, respectively). For sites exposed to the environment, fluorescence imaging indicated absence of microchannels at 24 hrs (Fig. 9b). For occluded sites, even though the microchannels remained open at 24 hrs, the fluorescent images indicated decreased fluorescence indicating partial closure of pores. This is further supported from the pore permeability index (PPI) values computed from the analysis of the images (Fig. 10). For example, for the site occluded with plastic film, pore permeability index (PPI) value decreased from an initial value of 11.7 to 3.7 (Fig. 10b & d). A similar trend was observed for occlusion with water, citrate buffer and phosphate buffer (data not shown).

Studies at further time points show the presence of microchannels even at 72 hrs *in vivo* under occluded conditions, which eventually closed by 120 hrs (Fig. 11).

DISCUSSION

Microneedles have been fabricated from a range of materials, such as silicon, glass, polymers and metals. However, due to potential issues such as breakage of the

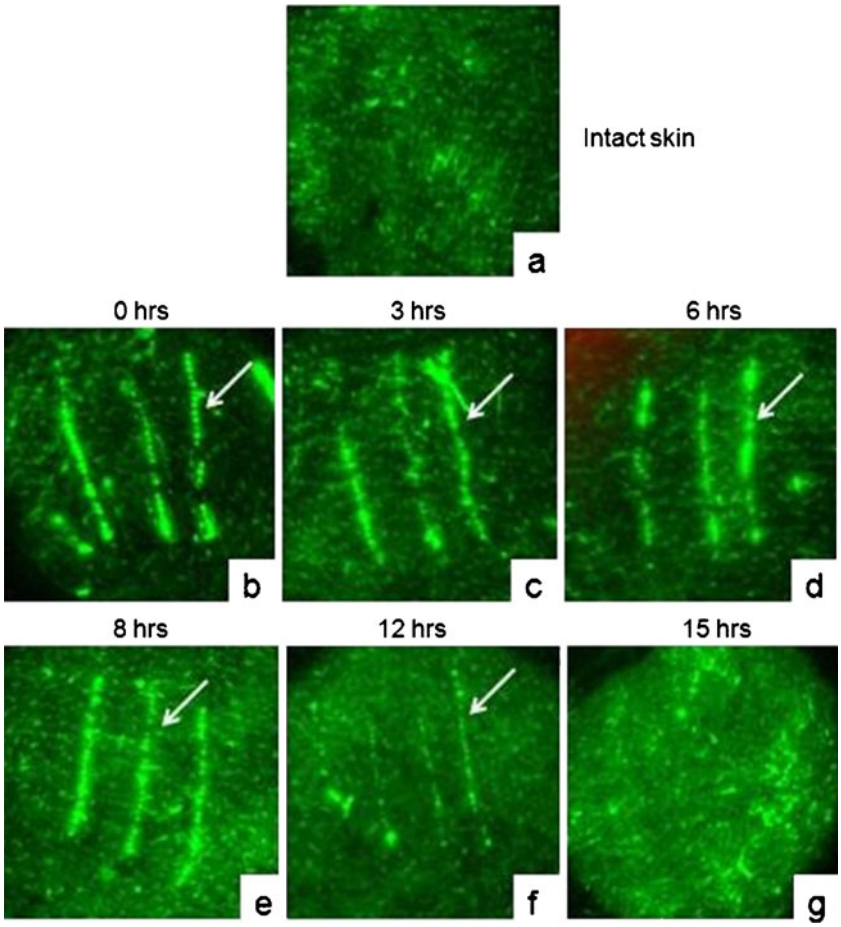

Fig. 8 Calcein imaging to study the kinetics of pore closure. Fluorescent images were taken for (**a**) intact skin and at (**b**) 0 hr, (**c**) 3 hrs, (**d**) 6 hrs, (**e**) 8 hrs, (**f**) 12 hrs and (**g**) 15 hrs after microporation. Pores closed by 15 hrs *in vivo* under non-occluded conditions.

needles in the skin, manufacturing costs and other complexities, microneedles made of biodegradable polymers have been explored (2,6). In this study, soluble microneedles made of a sugar (maltose) were employed. Fig. 2 shows the SEM images of maltose microneedles with an average length of 559 μm ± 14 μm. The sharp tips of the microneedles ensure the effective penetration of the microneedles past the stratum corneum barrier. These microneedles dissolve upon insertion into skin, resulting in hydrophilic channels which aid in transdermal drug

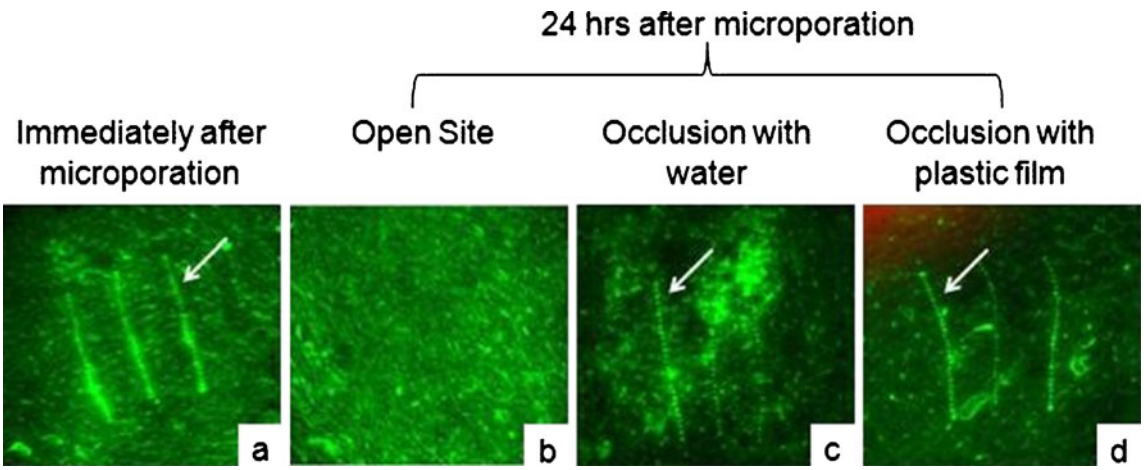

Fig. 9 Calcein imaging indicating the presence or absence of microchannels at 24 hrs after microporation. Microchannels were created with maltose microneedles (**a**) and subjected to different conditions. At 24 hrs after poration, microchannels were not observed for (**b**) open (non-occluded) site. However, microchannels were observed for sites (**c**) occluded with water and (**d**) occluded with a plastic film.

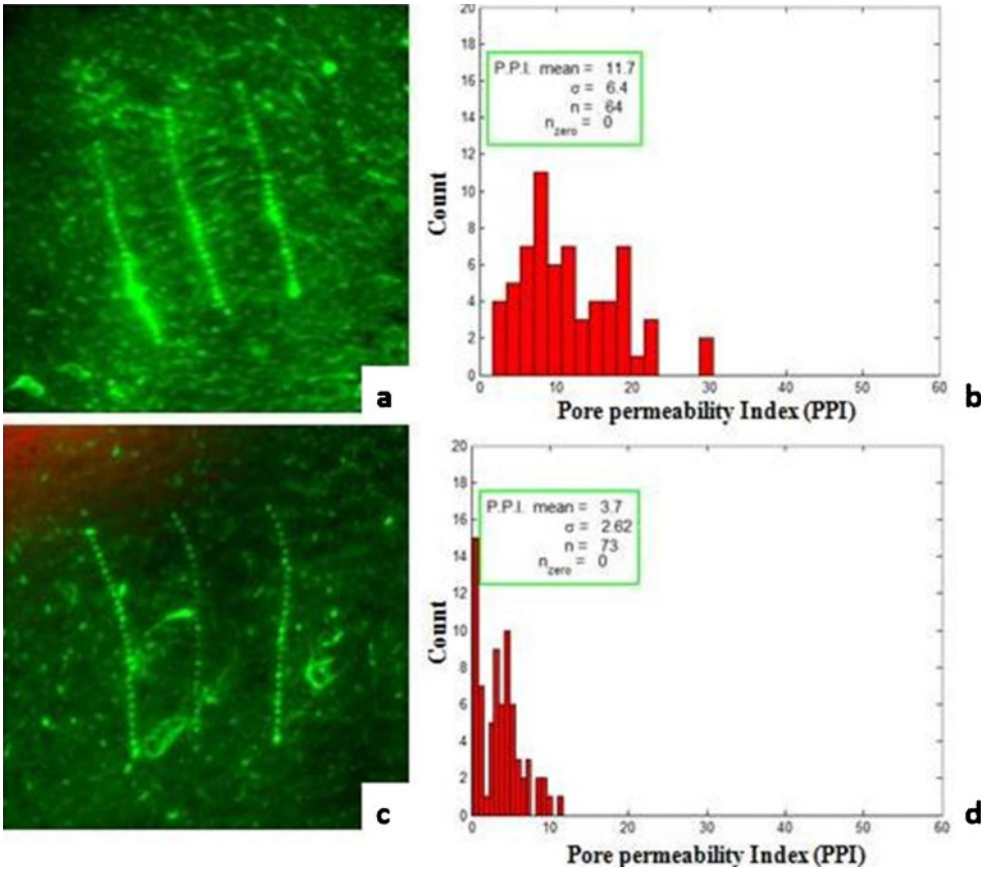

Fig. 10 Partial pore closure as indicated by calcein imaging: (**a**) fluorescent image showing microchannels immediately after poration and its corresponding (**b**) histogram showing the pore permeability values for freshly porated skin; (**c**) fluorescent image showing microchannels at 24 hrs when occluded with a plastic film with its corresponding (**d**) histogram.

delivery (2,11). Microchannels were effectively created as indicated by methylene blue staining (Fig. 3), confocal microscopy (Fig. 4) and histological sectioning (Fig. 5).

As discussed earlier, the dimensions of the created microchannels significantly depend on the geometry of the employed microneedles. Parameters such as the tip diameter, base width, length of the microneedle, type of microneedle (solid/hollow) and its mechanical strength play a critical role in the dimensions of the created microchannel. Al-Qallaf and Das have studied a varied range of geometries for investigating an optimal design for a microneedle (21,25). Also, the dimensions of the microchannels would vary according to the technology employed for microporation, such as electroporation, laser ablation and sonomacroporation.

Most studies reported in literature have characterized only the surface morphology of the microchannels, and relatively less literature is available on the characterization of the microchannel pathway created by the microneedles and their subsequent closure. It is important to consider issues such as pore closure while designing microneedle-based patches as it may have undesired implications. For

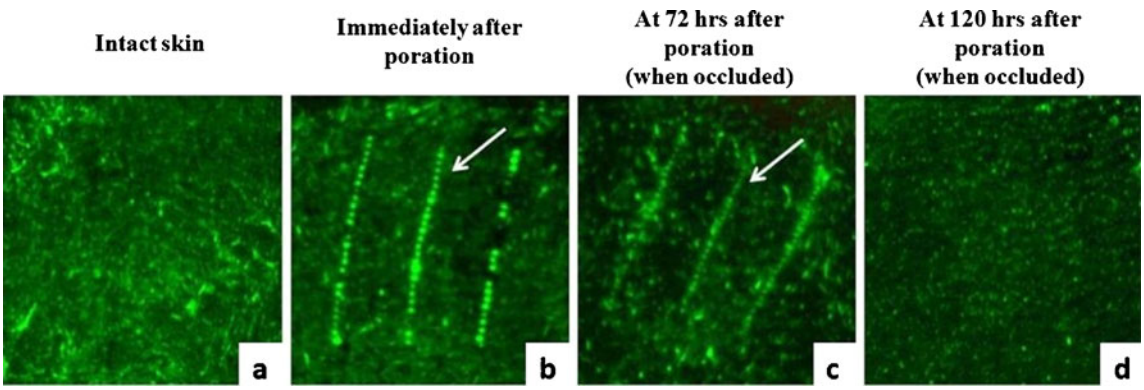

Fig. 11 Pore closure under occluded conditions (plastic film). (**a**) Intact skin before poration; (**b**) immediately after poration; (**c**) at 72 hrs after poration and (**d**) at 120 hrs after poration. *Arrow* indicates presence of microchannels.

example, if the pores close when the patch is applied on the skin, it may result in sub-therapeutic levels in the body. On the other hand, if pores remain open even after removal of the patch, it may result in problems such as irritation, infection and contamination of the site. Therefore, these studies were aimed at understanding pore closure following microporation.

The depth of the created microchannels was investigated by confocal microscopy with 0.2 μm-sized fluorescent particles. Upon application, the microparticles penetrate through the entire length of the microchannels, thus indicating their depth. A fluorescent solution, such as calcein, was not employed in order to avoid false interpretation of data due to diffusion of the dye past the microchannels. As can be seen in Fig. 4, the microparticles penetrated up to a depth of 160±20 μm, indicating the depth of the microchannels. Therefore, maltose microneedles with an average length of ~560 μm created microchannels with an average depth of 160±20 μm, and a surface diameter of ~60 μm. Histological examination of skin samples fixed immediately after poration further validated the data obtained from confocal microscopy. Figs. 5a–e indicate skin sections at varied depths from the skin surface. Methylene blue dye was imaged upto a depth of 160 μm, indicating the depth of the microchannels (Fig. 5d).

Having confirmed the creation of pores, the effect of different conditions on pore closure was investigated. The porated sites were either left open to the environment, occluded by a plastic film, occluded with citrate buffer (pH 4), occluded with PBS buffer (pH 7.4) or occluded with distilled water. The experimental conditions (as depicted by the schematic in Fig. 1) were set specifically to study the effect of occlusion and formulation pH on pore closure.

Transepidermal water loss (TEWL) measurements were employed as an indirect method to investigate the integrity of the stratum corneum barrier. Skin, being the protective barrier, protects the body from exogenous factors and at the same time also maintains skin hydration levels, thus resulting in less water loss from the body. Therefore, intact skin always has low TEWL values. In cases when the stratum corneum barrier is disrupted, the amount of water loss from the body increases, resulting in high TEWL values. This basic principle has been applied in several studies to study skin barrier function. In this study, TEWL values were taken as a supportive tool to study pore closure. Measurements taken on unperturbed skin were recorded as base values, and measurements taken immediately after microporation served as positive controls which indicated the presence of micropores. Low TEWL values around base values would indicate absence of pores, while high TEWL values around positive control values would indicate presence of pores.

In our studies, when we porate the skin, the amount of water loss from the body increases as indicated by the high TEWL values. Therefore, when this treated site is exposed to the environment, the increased water loss triggers barrier recovery by secreting organelles into the intercellular spaces. Menon *et al.* have reported that this further leads to secretion of nascent lamellar bodies which then transform into basic units in the mid-outer layers of the stratum corneum, thus resulting in barrier recovery. Basic unit structures were reported to appear in the lower SC by 1 hr, with higher levels by 3 hrs indicating better barrier homeostasis at the latter time point (19). Therefore, barrier function may return back to normal by 3 hrs as indicated by the TEWL values. TEWL values were recorded as a function of time to investigate the time taken for the values to fall back to base levels, indicating barrier integrity. For the open site, TEWL values returned to base values within 4 hrs of poration, indicating restored barrier function (Fig. 6). Gupta *et al.* have reported similar findings from skin impedance studies in human volunteers. They indicated that skin healed within 2 hrs under non-occluded conditions. However, when occluded, healing times were delayed but depended on the geometry of the microneedle employed, as indicated by low skin resistance values (22,23).

Studies were also performed to check for the effect of occlusion on barrier integrity of microporated skin. For the open site, at 24 hrs after poration, the TEWL values fell back to base values, indicating absence of micropores. However, for all the occluded conditions, the values remained high and comparable to control values, indicating presence of micropores (Fig. 7A). A similar trend was observed for the data obtained at 72 hrs after microporation (Fig. 7B). Therefore, as indicated by the TEWL values, pores remained viable for longer periods only under occluded conditions—both by a plastic film and by a solution. This was also confirmed by methylene blue staining at the end of the study. Fig. 7A (i) indicates the absence of micropores for the non-occluded site. However, for occluded sites, the micropores were visible even after 24 hrs as indicated by Figs. 7A (ii–iv), respectively.

Occlusion by impermeable membranes or solutions may cause a slight increase in skin hydration levels, which, in turn, may slightly affect TEWL values. Control studies indicated the same with a slight rise in TEWL values for untreated, occluded skin. However, the values were statistically lower than those obtained for the treated sites at the end of the study, thus indicating open pores. Also, from the TEWL data, it is indicative that pH did not have an effect on pore closure. To confirm this, a similar study was performed where treated sites were exposed to regular distilled water for 24 hrs. A similar trend was observed here as well where TEWL values remained high even after removal of the liquid reservoir patch (data not shown), thus

indicating that pores remain open when occluded by any solution, irrespective of pH. Therefore, when the treated sites are occluded by a plastic film or solution, the water loss is inhibited due to the occlusion, thereby maintaining skin water content and thus delaying barrier recovery. However, after removal of occlusion, TEWL recovered back to base values within 2 hrs (data not shown).

These results are supported by findings from Grubauer *et al.* (26) where they demonstrated the role of transepidermal water loss on barrier recovery. It was reported that when occluded with a nonpermeable membrane, barrier function did not recover normally. However, when occluded with a semi-permeable membrane, which allows only the permeation of water vapor, barrier function recovered back to normal, thus indicating that water gradient has a direct effect on barrier recovery. Occlusion in general has been shown to delay barrier recovery. Ahn *et al.* studied the effect of occlusion on skin barriers disrupted by different methods, such as tape stripping and application of surfactants (27). They reported that barrier recovery was delayed for 3 days under occlusion due to inhibition of formation of the lamellar bilayers in the stratum corneum. Barrier function was recovered only after removal of occlusion as indicated by the normal basic unit structure of the lamellar bilayers. The effects of some occlusive dressings on lamellar bodies in the stratum corneum have been reviewed by Kennish and Reidenberg (28). Menon *et al.* also reported that occluding disrupted skin barriers with an impermeable membrane resulted in a delay in barrier recovery associated with inhibition of lamellar body secretion (19). These lamellar bodies mediate transcutaneous water loss and thereby play an important role in barrier function (20). Therefore, transepidermal water loss may be a good indicator of barrier function in microneedle-treated skin.

Barrier recovery is an ongoing process which starts almost immediately after skin barrier disruption. Studies have shown that barrier recovery and epidermal calcium gradient restore in a parallel manner in compromised skin (29). Ahn *et al.* have suggested the possibility that occlusion with an artificial barrier would only delay barrier recovery

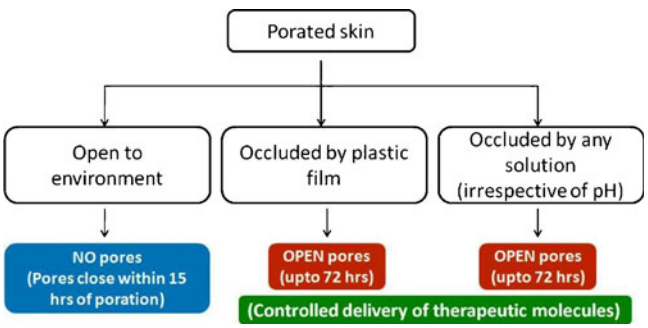

Fig. 12 Schematic showing the effect of different conditions on pore closure.

Table I Comparison of Reported Studies on Microchannels Created by Microneedles

Group	Model / Staining	TEWL	Calcein imaging	Pore permeability index (PPI)	Skin impedance
Haq *et al.*	Human study, Methylene blue staining; pores were observed and skin repair and resealing was apparent at 8–24 hrs post treatment	Microneedle length: 180 μm and 280 μm. TEWL values fell to baseline values within 24 hrs, however, not statistically significant when compared to control.	N/A	N/A	N/A
Gupta *et al.*	Human study; staining studies were not done	N/A	N/A	N/A	Skin healed within 2 hrs as indicated by impedance values.
Kalluri and Banga (this study)	Hairless rat model. Methylene blue staining; pores were created	Microneedle length: 500 μm TEWL values recovered within 3–4 hrs post treatment. Occlusion resulted in delay of barrier recovery as indicative by high TEWL values; statistically significant.	Direct visualization indicated complete pore closure within 15 hrs. Occlusion delayed pore closure for 72 hrs.	PPI values decreased as a function of time, indicating partial closure of pores.	N/A

by delaying restoration of the calcium gradient, which is then followed by normal recovery (27). Menon *et al.* have also reported that barrier disruption alters the epidermal calcium gradient, and its recovery is prevented by occlusion (29). However, Ahn *et al.* found that the epidermal calcium gradient was restored by 60 hrs under occluded conditions (27). It has been indicated that in murine epidermis, the initial barrier recovery phase, lasting 6 hrs, results in 50–60% recovery, which is then followed by the prolonged recovery phase (30,31). Even though the recovery can be delayed by factors discussed above, barrier recovery may progress at a slow rate. Therefore, even though pores remain open for a period of time, they might not have the same initial dimensions (depth and width), which may affect drug delivery of certain drug molecules.

It has been reported that occlusion of disrupted barrier artificially restores barrier function but inhibits barrier recovery (32). Therefore, calcein imaging was also performed for a more direct visualization of pore closure when subjected to the different test conditions. When the microneedle-treated site was exposed to the environment (no occlusion), pores closed partially by 12 hrs (Fig. 8f) as indicated by faint fluorescence, and they closed completely by 15 hrs *in vivo* (Fig. 8g). Therefore, it seems that even though barrier function is restored by 4 hrs *in vivo*, as indicated by TEWL values, it takes about 15 hrs for the pores to close completely. Calcein imaging studies with occlusion by water or plastic film further confirmed the presence of pores under occluded conditions (Fig. 9).

Fluorescent images were also analyzed using Fluoropore software, which measures the fluorescent intensity in and around each pore to give a value called the Pore Permeability Index (PPI). When occluded with a plastic film, though there was a decrease in the mean PPI from 11.7 to 3.7 at 24 hrs, pores remained viable (Fig. 10). Similar results were obtained for occlusion with water, citrate and phosphate buffers (data not shown). These findings indicate the possibility of partial closure of pores even under occlusion. Further studies were performed to study complete pore closure under occluded conditions. As seen in Fig. 11, pores remained open for up to 72 hrs (3 days) *in vivo*. However, they completely closed by 120 hrs (5 days).

Additionally, other factors such as ions have also been known to play an important role in barrier recovery. Excess calcium and potassium ions have been shown to delay barrier recovery in disrupted skin barriers (33–35). Strong bases, termed superbases due to their highly basic pH, have also been shown to alter skin pH, affect barrier function and delay barrier recovery. The acidic mantle of the stratum corneum layer is affected by a superbase-induced increase in pH, thereby altering barrier function (36–38). Therefore, several factors need to be considered when designing a microneedle patch. While some of these factors may be advantageous, others may have undesired implications.

This reversible nature of microchannel formation where pores close within 15 hrs of poration is very advantageous to microneedle technology and may aid in controlled delivery of therapeutic molecules (Fig. 12).

Since pore closure is an important aspect of microneedle technology, other groups have also tried to study this phenomenon by other techniques. The methods employed and the results obtained by two groups—Gupta *et al.* (22,23) and Haq *et al.* (24)—have been compiled and compared to our data in Table I.

CONCLUSIONS

In a hairless rat model, maltose microneedles penetrated the stratum corneum barrier and dissolved in skin, creating microchannels with an average surface diameter of 60 μm and a depth of 160±20 μm. When exposed to the environment, skin recovered its barrier function within 4 hrs as indicated by the transepidermal water loss measurements. However, direct superficial visualization by calcein imaging indicated that pores close slowly over about 15 hrs. When the treated sites were occluded with a solution, irrespective of pH, the microchannels remained open up to 72 hrs *in vivo*, as indicated by transepidermal water loss measurements, calcein imaging and methylene blue staining. The same phenomenon was observed when the treated sites were occluded with a water-vapor-impermeable plastic film. This pore closure behavior is likely to be advantageous for drug delivery, as pores will stay open while the patch is applied, allowing drug delivery. These pores start to close once the patch is removed, preventing possible infection of the porated site.

ACKNOWLEDGEMENTS

The authors would like to thank Dr. Chandrasekhar Kolli and David Farquhar for help with calcein imaging studies.

REFERENCES

1. Banga AK. Microporation applications for enhancing drug delivery. Expert Opin Drug Deliv. 2009;6:343–54.
2. Kolli CS, Banga AK. Characterization of solid maltose microneedles and their use for transdermal delivery. Pharm Res. 2008;25:104–13.
3. Cormier M, Johnson B, Ameri M, Nyam K, Libiran L, Zhang DD *et al.* Transdermal delivery of desmopressin using a coated microneedle array patch system. J Control Release. 2004;97:503–11.

4. Martanto W, Davis SP, Holiday NR, Wang J, Gill HS, Prausnitz MR. Transdermal delivery of insulin using microneedles *in vivo*. Pharm Res. 2004;21:947–52.
5. Davis SP, Martanto W, Allen MG, Prausnitz MR. Hollow metal microneedles for insulin delivery to diabetic rats. IEEE Trans Biomed Eng. 2005;52:909–15.
6. Park JH, Allen MG, Prausnitz MR. Biodegradable polymer microneedles: fabrication, mechanics and transdermal drug delivery. J Control Release. 2005;104:51–66.
7. Matriano JA, Cormier M, Johnson J, Young WA, Buttery M, Nyam K *et al.* Macroflux microprojection array patch technology: a new and efficient approach for intracutaneous immunization. Pharm Res. 2002;19:63–70.
8. Lin W, Cormier M, Samiee A, Griffin A, Johnson B, Teng CL *et al.* Transdermal delivery of antisense oligonucleotides with microprojection patch (Macroflux) technology. Pharm Res. 2001;18:1789–93.
9. Chabri F, Bouris K, Jones T, Barrow D, Hann A, Allender C *et al.* Microfabricated silicon microneedles for nonviral cutaneous gene delivery. Br J Dermatol. 2004;150:869–77.
10. McAllister DV, Wang PM, Davis SP, Park JH, Canatella PJ, Allen MG *et al.* Microfabricated needles for transdermal delivery of macromolecules and nanoparticles: fabrication methods and transport studies. Proc Natl Acad Sci USA. 2003;100: 13755–60.
11. Li G, Badkar A, Nema S, Kolli CS, Banga AK. *In vitro* transdermal delivery of therapeutic antibodies using maltose microneedles. Int J Pharm. 2009;368:109–15.
12. Widera G, Johnson J, Kim L, Libiran L, Nyam K, Daddona PE *et al.* Effect of delivery parameters on immunization to ovalbumin following intracutaneous administration by a coated microneedle array patch system. Vaccine. 2006;24:1653–64.
13. Teo MAL, Shearwood C, Ng KC, Lu J, Moochhala S. *In vitro* and *in vivo* characterization of MEMS microneedles. Biomed Microdevices. 2005;7:47–52.
14. Wang PM, Cornwell M, Hill J, Prausnitz MR. Precise microinjection into skin using hollow microneedles. J Invest Dermatol. 2006;126:1080–7.
15. Kalluri H, Banga AK. Microneedles and transdermal drug delivery. Journal of drug delivery science and technology. In print: 2009.
16. Teo AL, Shearwood C, Ng KC, Lu J, Moochhala S. Transdermal microneedles for drug delivery applications. Mater Sci Eng B. 2006.
17. Oh JH, Park HH, Do KY, Han M, Hyun DH, Kim CG *et al.* Influence of the delivery systems using a microneedle array on the permeation of a hydrophilic molecule, calcein. Eur J Pharm Biopharm. 2008;69:1040–5.
18. Mikszta JA, Alarcon JB, Brittingham JM, Sutter DE, Pettis RJ, Harvey NG. Improved genetic immunization via micromechanical disruption of skin-barrier function and targeted epidermal delivery. Nat Med. 2002;8:415–9.
19. Menon GK, Feingold KR, Elias PM. Lamellar body secretory response to barrier disruption. J Invest Dermatol. 1992;98:279–89.
20. Elias PM. Epidermal lipids, barrier function, and desquamation. J Invest Dermatol. 1983;80(Suppl):44s–9.
21. Al-Qallaf B, Das DB. Optimizing microneedle arrays for transdermal drug delivery: extension to non-square distribution of microneedles. J Drug Target. 2009;17:108–22.
22. Gupta J. Microneedles for transdermal drug delivery in human subjects, *School of Chemical and Biomolecular Engineering*, Vol. Ph.D. Dissertation, Georgia Institute of Technology, Atlanta; 2009. p. 198.
23. Gupta J, Andrews S, Gill HS, Prausnitz MR. Kinetics of skin resealing after insertion of microneedles in human subjects. New York: Controlled Release Society Annual Meeting; 2008.
24. Haq MI, Smith E, John DN, Kalavala M, Edwards C, Anstey A *et al.* Clinical administration of microneedles: skin puncture, pain and sensation. Biomed Microdevices. 2009;11:35–47.
25. Al-Qallaf B, Das DB. Optimizing microneedle arrays to increase skin permeability for transdermal drug delivery. Ann N Y Acad Sci. 2009;1161:83–94.
26. Grubauer G, Elias PM, Feingold KR. Transepidermal water loss: the signal for recovery of barrier structure and function. J Lipid Res. 1989;30:323–33.
27. Ahn SK, Jiang SJ, Hwang SM, Choi EH, Lee JS, Lee SH. Functional and structural changes of the epidermal barrier induced by various types of insults in hairless mice. Arch Dermatol Res. 2001;293:308–18.
28. Kennish L, Reidenberg B. A review of the effect of occlusive dressings on lamellar bodies in the stratum corneum and relevance to transdermal absorption. Dermatol Online J. 2005;11:7.
29. Menon GK, Elias PM, Feingold KR. Integrity of the permeability barrier is crucial for maintenance of the epidermal calcium gradient. Br J Dermatol. 1994;130:139–47.
30. Menon GK, Grayson S, Elias PM. Ionic calcium reservoirs in mammalian epidermis: ultrastructural localization by ion-capture cytochemistry. J Invest Dermatol. 1985;84:508–12.
31. Taljebini M, Warren R, Mao-Oiang M, Lane E, Elias PM, Feingold KR. Cutaneous permeability barrier repair following various types of insults: kinetics and effects of occlusion. Skin Pharmacol. 1996;9:111–9.
32. Jiang S, Koo SW, Lee SH. The morphologic changes in lamellar bodies and intercorneocyte lipids after tape stripping and occlusion with a water vapor-impermeable membrane. Arch Dermatol Res. 1998;290:145–51.
33. Mao-Qiang M, Mauro T, Bench G, Warren R, Elias PM, Feingold KR. Calcium and potassium inhibit barrier recovery after disruption, independent of the type of insult in hairless mice. Exp Dermatol. 1997;6:36–40.
34. Lee SH, Elias PM, Proksch E, Menon GK, Mao-Quiang M, Feingold KR. Calcium and potassium are important regulators of barrier homeostasis in murine epidermis. J Clin Invest. 1992;89: 530–8.
35. Lee SH, Elias PM, Feingold KR, Mauro T. A role for ions in barrier recovery after acute perturbation. J Invest Dermatol. 1994;102:976–9.
36. Hachem JP, Crumrine D, Fluhr J, Brown BE, Feingold KR, Elias PM. pH directly regulates epidermal permeability barrier homeostasis, and stratum corneum integrity/cohesion. J Invest Dermatol. 2003;121(2):345–53.
37. Fluhr JW, Mao-Qiang M, Brown BE, Hachem JP, Moskowitz DG, Demerjian M, Haftek M, Serre G, Crumrine D, Mauro TM, Elias PM, Feingold KR. Functional consequences of a neutral pH in neonatal rat stratum corneum. J Invest Dermatol. 2004;123 (1):140–50.
38. Hachem JP, Man MQ, Crumrine D, Uchida Y, Brown BE, Rogiers V, Roseeuw D, Feingold KR, Elias PM. Sustained serine proteases activity by prolonged increase in pH leads to degradation of lipid processing enzymes and profound alterations of barrier function and stratum corneum integrity. J Invest Dermatol. 2005;125(3):510–20.